IEEE Access
Multidisciplinary | Rapid Review | Open Access Journal

Received May 11, 2020, accepted May 21, 2020, date of publication May 26, 2020, date of current version June 8, 2020.

Digital Object Identifier 10.1109/ACCESS.2020.2997679

Frequency Domain Multi-Carrier Modulation Based on Prolate Spheroidal Wave Functions

HONGXING WANG, FAPING LU, CHUANHUI LIU, XIAO LIU, AND JIAFANG KANG
Department of Aeronautical Communication, Naval Aviation University, Yantai 264001, China
Key Laboratory on Signal and Information Processing of Shandong Province, Yantai 264001, China

Corresponding author: Faping Lu (lufaping@163.com)

This work was supported in part by the National Natural Science Foundation of China under Grant 6170012154, and in part by the Special Foundation Project of Taishan Scholar of Shandong Province under Grant ts20081130.

ABSTRACT A novel frequency domain multi-carrier modulation (MCM-FD) scheme is proposed based on prolate spheroidal wave functions (PSWFs) for reducing the high complexity in the conventional time domain PSWFs multi-carrier modulation (MCM-PSWFs-TD) schemes. By constructing the relationship between discrete representation and exponential function representation of MCM-PSWFs-TD signals, it can be observed that the orthogonality and parity symmetry of the waveforms of PSWFs in the frequency domain are the same as that in the time domain. Thus, the PSWFs signal can be divided into two groups based on their parity symmetry, while these two groups of PSWFs signals can be processed simultaneously. Based on this concept, signal waveforms with only half spectrum range are invoked in the process of information loading and signal detection for reducing the number of sampling points participated in the signal operation. Compared to the MCM-PSWFs-TD scheme, the proposed MCM-PSWFs-FD scheme is capable of significantly reducing the computational complexity without severely degrading the system performance, such as spectral efficiency (SE), bit error rate performance, signal energy concentration and peak-to-average power ratio (PAPR). Furthermore, the cyclic-prefix orthogonal frequency division multiplexing (CP-OFDM), OFDM with weighted overlap and add (WOLA-OFDM), filter OFDM (F-OFDM), universal filtered multi-carrier (UFMC), as well as the filter bank multi-carrier with offset quadrature amplitude modulation (FBMC-OQAM) are also demonstrated as benchmarks. Simulation results are provided for illustrating that the proposed MCM-PSWFs-FD scheme is capable of striking a favorable tradeoff between the computational complexity and the system performance (i.e. SE, out-of-band energy leakage, adjacent frequency band interference, and PAPR), while the signal waveform design of the MCM-PSWFs-FD scheme is also more concise and flexible than the benchmarks.

INDEX TERMS Prolate spheroidal wave functions, multi-carrier modulation, waveform design, time-frequency resource allocation, spectral efficiency.

I. INTRODUCTION

The next generation of mobile communication systems are expected to meet unprecedented high requirements for the ''quality'', ''quantity"'' and ''diversity'' of information transmission [1]–[3]. It requires more flexible new radio (NR), which can directly allocate resources in the two-dimensional (2D) space of time-frequency domain for obtaining flexible allocation and dynamic sharing of different types of time-frequency resources [4]–[7]. Prolate spheroidal wave functions (PSWFs), defined by Slepian and Pollak from the Bell Labs in1961 [8], which has many beneficial characteristics such as complete orthogonality, parity symmetry in waveform, high energy concentration in both time domain and frequency domain, flexibility and controllability in parameter setting (time-bandwidth product and spectrum), etc. Due to their beneficial characteristics, PSWFs can be directly designed in the 2D space of time-frequency domain, which can be viewed as a promising candidate for designing the signal waveform in the next-generation mobile communication systems [9], [10].

In recent decades, a variety of time domain multi-carrier modulation schemes based on PSWFs (MCM-PSWFs-TD) have been proposed, such as orthogonal PSWFs modulation method [11], pulse shape modulation based on PSWFs [12], [13], orthogonal carrier modulation based on PSWFs [14], orthogonal PSWFs modulation based on ternary coding [15], multidimensional constellation PSWFs

The associate editor coordinating the review of this manuscript and approving it for publication was Qilian Liang.

modulation [16], multidimensional coded modulation with PSWFs [17], non-orthogonal pulse shape modulation with PSWFs (NPSM-PSWFs)[18] and power domain NPSM-PSWFs [19], etc. The core idea of these modulation schemes is directly designing the PSWFs signal in the 2D space of time-frequency domain. By dividing the spectrum into multiple overlapping sub-bands, the PSWFs signals, which are orthogonal in the time domain while aliasing or overlapping in the frequency domain, are adopted for multiple parallelism transmission. Moreover, the MCM-PSWFs-TD scheme can concisely and flexibly design signal waveforms with high energy concentration (EC) and spectral efficiency (SE). Compared to the orthogonal frequency division multiplexing (OFDM) scheme, the SE of the MCM-PSWFs-TD scheme can approach 2Baud/Hz faster [19]. However, since the PSWFs have no closed-form/analytical expression, they are generated by numerical solutions in practical applications. In this case, the time-domain sampling rate of the numerical solution has to outclass the Nyquist sampling rate [20]. On the other hand, the MCM-PSWFs-TD scheme processes signal in the time domain, while all the signal sampling points are required for operating. Thus, the MCM-PSWFs-TD scheme is of a high complexity, which in turn, severely increases the signal processing delay and reduces the overall transmission efficiency of the communication system. Meanwhile, the IFFT/FFT signal processing modules, which are widely utilized in LTE and 5G, cannot be directly adopted in the MCM-PSWFs-TD schemes. Hence, in this paper, we aim for designing an alternative solution of waveform design in some 5G scenarios by proposing a novel MCM-PSWFs scheme. Additionally, our previous work [21] separately processes odd symmetric and even symmetric waveforms of PSWFs based on their parity symmetry in the time domain, which is capable of effectively reducing the complexity of the generation and detection of signals. Meanwhile, this also provides a novel solution for reducing the complexity of MCM-PSWFs system.

In an effort to tackle the aforementioned bottleneck problem of the MCM-PSWFs-TD scheme, we proposed a novel frequency domain multi-carrier modulation based on PSWFs (MCM-PSWFs-FD) with the aid of IFFT/FFT method, which switches the signal processing from the time domain to the frequency domain. More specifically, in the first step, the discrete representation of PSWFs signals in the frequency domain, as well as the relationship between discrete representation and exponential function of the MCM-PSWFs-TD signal are systematically analyzed based on the complete orthogonality and parity symmetry of PSWFs signal in the frequency domain [22] for reducing the number of signal sampling points participated in the signal operation. In the second step, in order to effectively reduce the number of sampling points required for effective representing the PSWFs signals, the PSWFs signals in frequency domain are discretely expressed by extracting the imaginary part of the frequency domain signal to represent the time domain odd symmetric signal while the real part represents the time domain even symmetric signal. In the third step, the odd symmetric and even symmetric signals are individually processed according to the parity symmetry of PSWFs signals in the frequency domain. Based on which, the signal waveform with half spectrum range is invoked in the process of information loading and frequency domain signal detection. Theoretical analysis and numerical results demonstrate that the proposed MCM-PSWFs-FD scheme can significantly reduce the number of signal sampling points involved in the signal processing compared to the MCM-PSWFs-TD scheme. Additionally, the MCM-PSWFs-FD scheme outperforms the existing MCM-PSWFs-TD schemes in terms of complexity without severely degrading the system performance, such as SE, EC of the modulation signal, signal peak-to-average power ratio (PAPR), bit error rate (BER) performance.

Since the proposed MCM-PSWFs-FD scheme adopts the same IFFT/FFT method with some 5G/B5G candidate modulation schemes, such as the cyclic-prefix OFDM (CP-OFDM), OFDM with weighted overlap and add (WOLA-OFDM) [23], filtered OFDM (F-OFDM) [24], universal filtered multi-carrier (UFMC) [25], [26] and the filter bank multi-carrier with offset quadrature amplitude modulation (FBMC-OQAM) [27], [28], the system performance of the proposed MCM-PSWFs-FD scheme is compared to the aforementioned candidate modulation schemes. Finally, the advantages of the proposed MCM-PSWFs-FD scheme compared to the benchmarks are as follows:

1) Compared to the CP-OFDM, WOLA-OFDM, F-OFDM, and UFMC schemes, the signal waveform design of the MCM-PSWFs-FD scheme is more concise and flexible, with higher EC and SE, lower adjacent frequency band interference and PAPR;

2) Compared to the FBMC-OQAM scheme, which is highly desired both in academia and industry, the MCM-PSWFs-FD scheme is capable of attaining lower PAPR while obtaining higher SE in the scenario that the number of symbol periods is small. It is worth noting that the FBMC-OQAM scheme outperforms the MCM-PSWFs-FD scheme in term of the PSD properties and adjacent frequency band interference, while strike a higher SE in the condition that the number of transmission symbol period is large.

The remaining sections are organized as follows. The relationship between discrete representation and exponential function representation of MCM-PSWFs-TD signals, the discrete representation of the PSWF signals in frequency domain, and the system models of the proposed MCM-PSWFs-FD scheme are presented in Section II. Afterward, Sections III provides the comparison and analysis between the proposed MCM-PSWFs-FD scheme and the aforementioned MCM schemes adopt the IFFT/FFT method in terms of power spectral density (PSD), SE, BER, PAPR, and computational complexity. Then, numerical results about the PSD, PAPR, BER performance, and adjacent frequency band interference of the proposed MCM-PSWFs-FD scheme are presented and discussed in Section IV. Finally, Section V concludes the paper.

II. FREQUENCY DOMAIN MULTI-CARRIER MODULATION BASED ON PSWFs

As non-periodic and frequency continuous signals, it is non-trivial to represent the PSWFs by explicating their expressions in the time domain and frequency domain since the PSWFs have no closed-form/analytical expression. In the MCM-PSWFs-TD scheme, the PSWFs signals are denoted by discrete-time representation. It is an open question whether the modulated PSWFs signals can be discretely represented in the frequency domain and the signal processing can be performed in the frequency domain for reducing the system complexity. Therefore, in this section, we first analyze the discrete-frequency representation of PSWFs signal, as well as the relationship between the discrete-time representation and exponential function representation of the MCM-PSWFs-TD signal. Secondly, we propose the MCM-PSWFs-FD scheme, which extends the signal processing from the time domain to the frequency domain for reducing the system complexity.

A. THE DISCRETE REPRESENTATION OF MODULATION SIGNAL

Let us denote the symbol period by T(s), the total number of symbol periods by Q. There are L sub-bands with a bandwidth of $B_l, l \in [1, L]$ in spectrum range $[f_0 - B/2, f_0 + B/2]$(Hz) while the overlapping degree in frequency domain between adjacent sub-bands is 0. Thus, the time-bandwidth product for the PSWFs signals in the l-th sub-band can be expressed as $c_l = B_l T$(Hz · s). In the symbol period $q \in [1, Q]$, the equivalent low-pass signal of the MCM-PSWFs-TD scheme with pulse amplitude modulation (PAM) constellation [11]–[19] in spectrum range $[-B/2, B/2]$(Hz) can be uniformly expressed as

$$s_q(t) = \sum_{l=1}^{L} \sum_{i=0}^{c_l - k_l - 1} x_{q,l,i} \varphi_{q,l,i}(c_l, t) e^{j2\pi(\gamma_l - B/2)t}, \quad (1)$$

where $\gamma_1 - B/2 = B_1/2 - B/2, \gamma_{l>1} - B/2 = \sum_{k=1}^{l-1}(B_k + B_{k+1}/2) - B/2$ represents the center frequency of the l-th sub-bands, $\varphi_{q,l,i}(c_l, t)$ denotes the PSWFs signal, whose time-frequency product is c_l, the spectrum range is $[-B_l/2, B_l/2]$(Hz) and the transmitted symbol is $x_{q,l,i} = x_{q,l,i,I} + i x_{q,l,i,Q}$.

In order to guarantee the energy concentration of the modulation signal, in the MCM-PSWFs-TD scheme, the former $c_l - k_l, k_l \geq k_{l,\min}, l \in [1, L]$ order PSWFs signals are selected for information transmission. The value $k_{l,\min}$ has to obey $k_{l,\min} \approx \lceil \ln\left(1/\lambda_{l,i} - 1\right) \log(2\sqrt{\pi c_l})/\pi^2 \rceil$, where $\lambda_{l,i}$ represents the energy concentration ratio of the $i \in [0, c_l - 1]$ order PSWFs signal [29]. In the practical applications, in order to guarantee that the modulation signal has low out-of-band (OOB) energy leakage for reducing the adjacent frequency band interference, the energy concentration ratio $\lambda_{l,i}$ has to satisfy that $\lambda_{l,i} \geq 99.9\%$ (30dB).

Denote the sampling rate in the time domain as $f_s = 1/\Delta t > B$, the discrete-time PSWFs signals can be given by $\varphi'_{q,l,i}(c_l, t_h) = \varphi_{q,l,i}(c_l, t_h) e^{j2\pi(\gamma_l - B/2)t_h} \in \mathbb{C}^{N_T \times 1}, t_h = h\Delta t, h = 0, 1, \cdots, N_T - 1, N_T = QTf_s > QTB$. According to (1), the modulation signal generation matrix $\mathbf{G} \in \mathbb{C}^{N_T \times Q(\sum_L c_l - k_l)}$ and transmission symbol $\mathbf{x} \in \mathbb{C}^{Q(\sum_L c_l - k_l) \times 1}$ of Q symbol periods and L sub-bands are formulated as

$$\begin{aligned} \mathbf{G} &= [\varphi'_{1,0,0} \cdots \varphi'_{1,0,c_0-k_0-1} \varphi'_{1,1,0} \cdots \varphi'_{Q,L,c_L-k_L-1}], \\ \mathbf{x} &= [x_{1,0,0} \cdots x_{1,0,c_0-k_0-1} x_{1,1,0} \cdots x_{Q,L,c_L-k_L-1}]. \end{aligned} \quad (2)$$

The corresponding discrete-time representation of the signal $\mathbf{s} \in \mathbb{C}^{N_T \times 1}$ can be expressed as $\mathbf{s} = \mathbf{G}\mathbf{x}$.

1) DISCRETE-FREQUENCY REPRESENTATION OF PSWFs SIGNALS

According to the definition of Fourier series, the PSWFs signal $\varphi_{q,l,i}(c_l, t)$ can be expressed as

$$\varphi_{q,l,i}(c_l, t) = a_{q,l,i,0}/2 + \sum_{n=1}^{\infty} \begin{pmatrix} a_{q,l,i,n} \cos(n\Omega t) \\ + b_{q,l,i,n} \sin(n\Omega t) \end{pmatrix}, \quad (3)$$

where $a_{q,l,i,0}/2 = \int_T \varphi_{q,l,i}(t) dt/T$ represents the direct component, Ω denotes the fundamental frequency, while $a_{q,l,i,n}, b_{q,l,i,n}$ indicate the component coefficient which can be expressed as

$$\begin{aligned} a_{q,l,i,n} &= \frac{2}{T} \int_T \varphi_{q,l,i}(c_l, t) \cos(n\Omega t) dt, \\ b_{q,l,i,n} &= \frac{2}{T} \int_T \varphi_{q,l,i}(c_l, t) \sin(n\Omega t) dt. \end{aligned} \quad (4)$$

It has been proved that the PSWFs are with the beneficial characteristics of acting as the optimal band-limit function set. The energy of PSWFs signals is uttermost concentrated in the spectral range of $[-B_l/2, B_l/2]$(Hz) [8], [10]. Thus, the number of fundamental frequency in the equation (3) is $N_F = 2\pi B_l/\Omega + 1 = B_l T + 1 = c_l + 1$.

Additionally, since the complete orthogonality of the PSWFs signal is also proved in the frequency domain while its spatial dimension in frequency domain is c_l [22], no loss of information will be generated by representing PSWFs signals with $c_l + 1$ fundamental components. Therefore, the PSWFs signals can be effectively represented in the frequency domain by $c_l + 1$ discrete frequencies with a frequency interval of $F = 1/T$(Hz). Correspondingly, the required sampling points for representing a baseband PSWFs signal with Q symbol periods and L sub-bands can be calculated as $N_F = Q(TB + 1) < N_T$.

2) EXPONENTIAL FUNCTION REPRESENTATION OF THE MODULATION SIGNAL

According to (2) - (4), the modulation signal in the q-th symbol period can be expressed as

$$s_q(t) = \sum_{l=1}^{L} \sum_{i=0}^{c_l - k_l - 1} \sum_{v=-c_l/2}^{c_l/2} a_{l,v,i} e^{j2\pi(\gamma_l - B/2 + v/T)t} x_{q,l,i}, \quad (5)$$

where $a_{l,v,i}$ represents the coefficient of $\varphi_{q,l,i}(c_l, t)$ at frequency v/T. Furthermore, with the sampling rate $f_s = N_{FFT}/T = N_T/T \geq \sum_L B_l$, we deduce that the exponential summation corresponds to an N_{FFT} point inverse discrete Fourier transform (DFT). Thus, the sampled version of (5), $\mathbf{s}_q \in \mathbb{C}^{N_{FFT}\times 1}$, can be expressed as (6), shown at the bottom of this page.

According to (3) - (6), the modulation signal is capable of being generated in the frequency domain. Additionally, the time domain waveform can be obtained by an inverse DFT.

Overall, the modulation signal of the MCM-PSWFs-TD scheme is capable of being processed in the frequency domain while the IFFT/FFT method can be adopted for obtaining the time domain (or frequency domain) signal waveform of the modulation signal. Additionally, in contrast to the signal processing in the time domain, signal processing in the frequency domain can effectively reduce the number of signal sampling points involved in the signal operation, which can shed light on the possibility of reducing signal processing complexity.

B. THE PROPOSED MCM-PSWFs-FD SCHEME

With the advantage that the discrete-frequency representation of the PSWFs signals requires fewer sampling points than the conventional methods, fully reap the parity symmetry of the PSWFs signals in the frequency domain for reducing the number of signal sampling points involved in the signal operation is a significant breakthrough for further reducing the system complexity.

Firstly, we can observe from the parity symmetry property of the PSWFs signal waveform that, the signal waveforms of the entire spectrum range can be obtained if only the signal waveforms of the half spectrum range are known in the frequency domain. If a modulation signal of the half spectrum range is generated first, then the modulation signal of the entire spectrum range can be generated by leveraging the symmetric extension. In this case, only signal waveforms of the half spectrum range are involved in the signal operation, which indicates that the number of signal sampling points involved in the signal operation is reduced.

Secondly, according to the definition of Fourier transform (FT), it reveals the relationship between the FT of the odd symmetric PSWFs signal $\varphi_O(t)$ and the even symmetric PSWFs signal $\varphi_E(t)$ as (7), shown at the bottom of this page.

According to (7), the real part of the PSWFs signal of odd symmetric after FT is 0 while the imaginary part performs as odd symmetry. In contrast, the real part of the PSWFs signal of even symmetric after FT performs as even symmetry while the imaginary part is 0. Additionally, the PSWFs signal has to satisfy $< \mathrm{Re}[\psi_E(jw)], \mathrm{Im}[\psi_O(jw)] >= 0$. This phenomenon indicates that the waveforms of PSWFs are also with orthogonality and parity symmetry in the frequency domain (consistent with the conclusion of [22]). A complete set of orthogonal bases constructed by PSWFs signals can be obtained and processed as a real form in the frequency domain by extracting the imaginary part (real part) of the signal after FT of the time domain odd symmetric (even symmetric) signal, i.e., $\psi'_O(jw) = \mathrm{Im}\{\psi_O(jw)\}, \psi'_E(jw) = \mathrm{Re}\{\psi_E(jw)\}$.

Furthermore, it can be observed from the signal multiplication property that, when multiplying PSWFs signals with the same parity symmetry in the frequency domain, the multiplied signal has the same shape and the same symbol on both sides of the signal center frequency. Therefore, the cross-correlation values of PSWFs signal with the same parity symmetry in the frequency domain satisfy the relationship as (8), shown at the bottom of this page.

$$\mathbf{s}_q = \underbrace{\mathbf{W}^H_{N_{FFT}} \begin{bmatrix} \cdots 0 & \overbrace{\begin{matrix} a_{1,-c_1/2,0}x_{q,0,0} \\ + \\ a_{1,-c_1/2,1}x_{q,0,1} \\ + \\ \vdots \\ a_{1,-c_1/2c_1-k_1-1}x_{q,0,c_1-k_1-1} \end{matrix}}^{\text{Band 1}} & \cdots\cdots\cdots & \overbrace{\begin{matrix} a_{L,c_L/2,0}x_{q,L,0} \\ + \\ a_{L,c_L/2,1}x_{q,L,1} \\ + \\ \vdots \\ a_{L,c_L/2,c_L-k_L-1}x_{q,L,c_L-k_L-1} \end{matrix}}^{\text{Band } L} & 0 \cdots \end{bmatrix}}_{\text{IFFT}}. \tag{6}$$

$$\begin{aligned} \psi_O(jw) &= \int_{-\infty}^{\infty} \varphi_O(t) e^{-jwt} dt = i \int_{-\infty}^{\infty} \varphi_O(t) \sin(wt) dt = -\psi_O(-jw), \\ \psi_E(jw) &= \int_{-\infty}^{\infty} \varphi_E(t) e^{-jwt} dt = \int_{-\infty}^{\infty} \varphi_E(t) cos(wt) dt = \psi_E(-jw). \end{aligned} \tag{7}$$

$$\gamma_{l,m,k} = \begin{cases} \int_{-B_l/2}^{B_l/2} \psi'_{l,O,m}(c_l, jw)\psi'_{l,O,k}(c_l, jw)dw = 2\int_0^{B_l/2} \psi'_{l,O,m}(c_l, jw)\psi'_{l,O,k}(c_l, jw)dw, \\ \int_{-B_l/2}^{B_l/2} \psi'_{l,E,m}(c_l, jw)\psi'_{l,E,k}(c_l, jw)dw = 2\int_0^{B_l/2} \psi'_{l,E,m}(c_l, jw)\psi'_{l,E,k}(c_l, jw)dw. \end{cases} \tag{8}$$

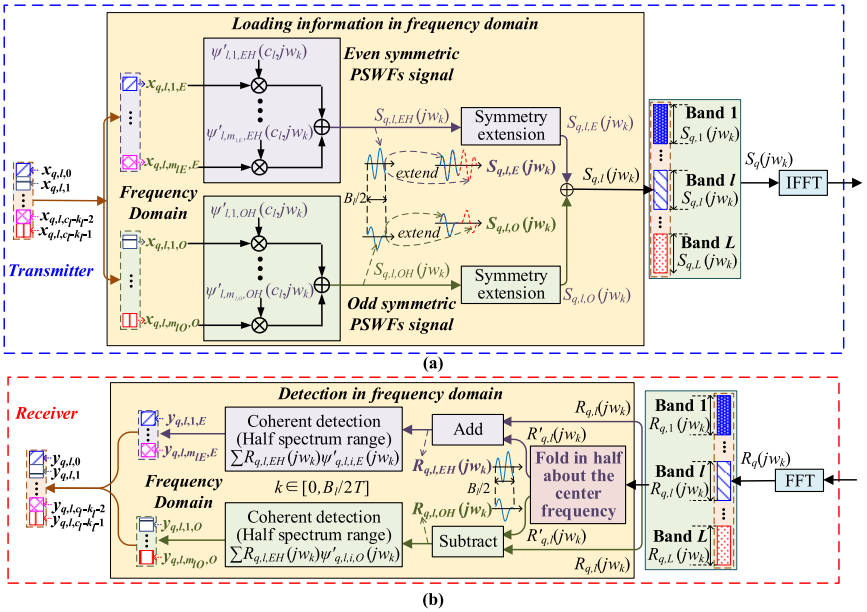

FIGURE 1. Block diagram of the MCM-PSWFs-FD with (a) block diagram of transmitter (b) block diagram of receiver.

The cross-correlation values of the PSWFs signals with the same parity symmetry in the bandwidth of $[-B_l/2, B_l/2]$ are twice that in the bandwidth of $[0, B_l/2]$ according to (8). If $\psi'_{O,m}(c, jw)$, $\psi'_{O,k}(c, jw)$, $m \neq k$ is orthogonal to each other in the bandwidth of $[-B_l/2, B_l/2]$, these signals are also mutually orthogonal in the bandwidth of $[0, B_l/2]$. In other words, the signals with the same parity symmetry have the same orthogonality over the half spectrum range and the entire spectrum range.

Therefore, the core idea of the MCM-PSWFs-FD scheme is that the PSWFs signals are partitioned into two groups (odd symmetric and even symmetric) according to the parity symmetry of the waveforms of PSWFs in the frequency domain. Signal waveforms of the half spectrum range are invoked in the process of information loading and signal detection in frequency domain. Fig. 1 illustrates the architecture of the proposed MCM-PSWFs-FD scheme, in which the half spectrum range modulation signals of odd symmetric and even symmetric are firstly produced for different sub-bands at the transmitting terminal. Then the time-domain modulation signal waveforms of the entire spectrum range are generated by invoking the symmetric extension, superposition, IFFT, etc. At the receiving terminal, the odd symmetric and even symmetric modulation signals of different sub-bands are separated by leveraging the FFT, signal folding, symmetric value superposition averaging, etc. Thus, these signals are detected in the frequency domain by utilizing the signal waveforms of the half spectrum range.

1) AT THE TRANSMITTING TERMINAL

The MCM-PSWFs-FD modulation signals are generated according to Fig. 1(a). More particularly:

Step 1: The modulation symbols $x_{q,l,i}, i \in [0, c_l - k_l - 1], l \in [1, L]$ are partitioned into two groups $x_{q,l,i,E}$, $i \in [1, m_{l,E}]$, $x_{q,l,i,O}$, $i \in [1, m_{l,O}]$ according to the number $m_{l,O}$, $m_{l,E}$ of the odd symmetric and even-symmetric PSWFs signals.

Step 2: Generate the modulation signal of the half spectrum range $S_{q,l,OH}(jw_k)$, $S_{q,l,EH}(jw_k)$, $w_k = -\lfloor B_l T/2 \rfloor + k/T, k = 0, 1, \cdots, \lfloor B_l T/2 \rfloor$, which can be calculated as follows

$$S_{q,l,OH}(jw_k) = \sum_{i=1}^{m_{l,O}} \psi'_{l,i,OH}(c_l, jw_k) x_{q,l,i,O},$$
$$S_{q,l,EH}(jw_k) = \sum_{i=1}^{m_{l,E}} \psi'_{l,i,EH}(c_l, jw_k) x_{q,l,i,E}, \quad (9)$$

where $\psi'_{l,i,OH}(c_l, jw_k)$, $\psi'_{l,i,EH}(c_l, jw_k)$ represent the odd symmetric and even symmetric discrete-frequency representation of the PSWFs signals, respectively.

Step 3: Generate the modulation signal of the entire spectrum range $S_{q,l,O}(jw_k), S_{q,l,E}(jw_k), k = 0, 1, \cdots, \lfloor B_l T \rfloor$ by invoking the symmetric extension. Obtain the l-th sub-band discrete-frequency modulation signal $S_{q,l}(jw_k) = S_{q,l,O}(jw_k) + S_{q,l,E}(jw_k)$ by linearly superimposing $S_{q,l,O}(jw_k)$ and $S_{q,l,E}(jw_k)$.

Step 4: Obtain the discrete-frequency signal $S_q(jw_k)$ of the MCM-PSWFs-FD scheme by sorting the modulation signal $S_{q,l}(jw_k), l \in [1, L]$ according to the order of sub-band $1 \to L$. Generate the time-domain waveform $s_q(t_h)$ of $S_q(jw_k)$ through IFFT processing while satisfying $t_h = (q-1)T + h\Delta t, h = 0, 1, \cdots, N_T - 1, N_T = N_{FFT} \geqslant N_F$.

2) AT THE RECEIVING TERMINAL

The demodulation and detection process of the MCM-PSWFs-FD scheme is demonstrated in Fig. 1 (b). More particularly:

Step 1: Obtain the discrete-frequency signal $R_q(jw_k)$, $l \in [1, L]$ by leveraging the FFT process. Separate the signals $R_{q,l}(jw_k)$ of different sub-band according to their order.

Step 2: Obtain the signal $R'_{q,l}(jw_k)$, $w_k = -\lfloor B_l T/2 \rfloor + k/T, k = 0, 1, \cdots, \lfloor B_l T/2 \rfloor, l \in [1, L]$ by folding signal $R_{q,l}(jw_k)$ about the center frequency of the l-th sub-band. Extract the odd symmetric and even symmetric signals $R_{q,l,OH}(jw_k), R_{q,l,EH}(jw_k)$ by performing subtraction and summation operations on $R_{q,l}(jw_k), R'_{q,l}(jw_k)$, respectively. The odd symmetric and even symmetric signals can be calculated as follows

$$\begin{aligned} R_{q,l,OH}(jw_k) &= R_{q,l}(jw_k) - R'_{q,l}(jw_k), \\ R_{q,l,EH}(jw_k) &= R_{q,l}(jw_k) + R'_{q,l}(jw_k). \end{aligned} \tag{10}$$

Step 3: Calculate the detection statistics of the different order PSWFs signals according to the following equations

$$\begin{aligned} E_{q,l,i,O,i\in[1,m_{l,O}]} &= \sum_{k=0}^{\lfloor B_l T/2 \rfloor} R_{q,l,OH}(jw_k)\psi'_{l,i,OH}(c_l, jw_k), \\ E_{q,l,i,E,i\in[1,m_{l,E}]} &= \sum_{k=0}^{\lfloor B_l T/2 \rfloor} R_{q,l,EH}(jw_k)\psi'_{l,i,EH}(c_l, jw_k). \end{aligned} \tag{11}$$

Step 4: Judge the statistical detection volume $E_{q,l,i,O}, i \in [1, m_{l,E}], E_{q,l,i,E}, i \in [1, m_{l,O}]$ and complete the signal detection of the PSWFs signals according to the decision rules.

C. BRIEF SUMMARY

1) COMPUTATIONAL COMPLEXITY

We leverage the complex multiplications (CMs) as the measurement criteria for analyzing the complexity of the MCM-PSWFs-FD scheme. Without loss of generality, it is assumed that $Q = 1, L = 1$, and the spectrum range and time-bandwidth product of PSWFs signal are $[0, B/2]$(Hz), $c = BT$(Hz $\cdot$ s), respectively. According to (2), (5) and (6), the time domain sampling points of the PSWFs signals are $N_T = VTB = Vc, V > 1$, while the frequency domain sampling points are $N_F = c + 1, c \geqslant 2$. Then, according to the basic principle of the MCM-PSWFs-TD scheme, the number of CMs for information loading and signal detection is $C_{\text{MCM - PSWFs - TD}} = 2Vc(c-k), k \geq k_{min}$. On the other hand, according to the basic principle of the MCM-PSWFs-FD scheme, its CMs mainly derives from information loading, detection and IFFT/FFT processing. The specific number of CMs in the MCM-PSWFs-FD is calculated as $C_{\text{MCM - PSWFs - FD}} = (c+1)(c-k) + C_{\text{IFFT}} + C_{\text{FFT}}$, $C_{\text{IFFT}} = C_{\text{FFT}} = [(c+1)\log_2(c+1)]/2$. In order to intuitively illustrate the advantages of the proposed method in terms of the complexity, here we denote that

$$\eta = \frac{C_{\text{MCM - PSWFs - TD}} - C_{\text{MCM - PSWFs - FD}}}{C_{\text{MCM - PSWFs - TD}}} \times 100\%. \tag{12}$$

It reveals in (12) that, compared to the MCM-PSWFs-TD scheme, the MCM-PSWFs-FD scheme can effectively reduce the computational complexity. It is also shown in (12) that, the decreased degree of the computational complexity constantly increases with the rising of c. Especially, when c large enough, the MCM-PSWFs-FD scheme is can greatly reduce the system complexity. Additionally, there are 12 subcarriers for each resource block in the LTE systems, which indicates that $c \geqslant 12$. To be more precise, when $V = 1, c = 12$ and $k = 3$, the value $\eta = 23.6\%$, which means that the system complexity is reduced by 23.6%; when $c = 96$ and $k = 2$, the value $\eta = 45.9\%$, which means that the system complexity is reduced by 45.9%.

2) SPECTRAL EFFICIENCY

It is demonstrated in (2), (3) and (5) that the MCM-PSWFs-FD signal is the mapping of the MCM-PSWFs-TD signal within the design bandwidth. Both two kind of signals have the same time width, bandwidth, and the number of PSWFs signals. Therefore, the MCM-PSWFs-FD scheme can also directly design signals in the 2D space of time-frequency domain while obtain the same SE with the MCM-PSWFs-TD scheme. Assume that the number of PSWFs signals is $BT - k, k \geqslant k_{\min}$ and PAM is M-ary, the SE of the MCM-PSWFs-FD scheme can be expressed as

$$SE = \frac{2\left[(BT-k)\log_2 M\right]}{BT} \quad \text{(bit/s/Hz)}. \tag{13}$$

As it is revealed in (13), the SE of the MCM-PSWFs-FD scheme is related to the time-bandwidth product BT and the value of k. As time-bandwidth product BT increases and value k decreases, the SE increases continuously.

3) ENERGY CONCENTRATION, PAPR AND BER PERFORMANCE

The energy concentration of the MCM-PSWFs-FD signals with IFFT/FFT is slightly lower than that of the MCM-PSWFs-TD signals. However, in the condition that the EC ratio of modulation signal is larger than 99.9%, the EC ratio gap between the MCM-PSWFs-FD scheme and the MCM-PSWFs-TD scheme in the design bandwidth is less than 10^{-3}, which is negligible. Under the AWGN channel conditions, when $c = 36\text{Hz} \cdot \text{s}, B = 0.54\text{MHz}, k = 3$ (the choice of parameter k is shown in Fig. 3(a)), the PSD, complementary cumulative distribution function (CCDF) and BER performance of the MCM-PSWFs-FD scheme are illustrated in Fig. 2. Simulation results are provided to demonstrate that the MCM-PSWFs-FD scheme and the MCM-PSWFs-TD scheme have the same PAPR and BER performance, and the EC ratio gap between modulation signals is 10^{-4} magnitude order, which is negligible.

According to the above analysis, compared to the MCM-PSWFs-TD scheme, the MCM-PSWFs-FD scheme can reduce the computational complexity from $O(2Vc^2)$ to $O(c^2 + c\log_2 c)$ without severely degrading the system performance, such as SE, signal EC, PAPR and BER performance. Additionally, since the MCM-PSWFs-FD scheme leverages the IFFT/FFT method, it can be applied to the communication systems such as Wi-Fi, LTE and 5G [30], [31].

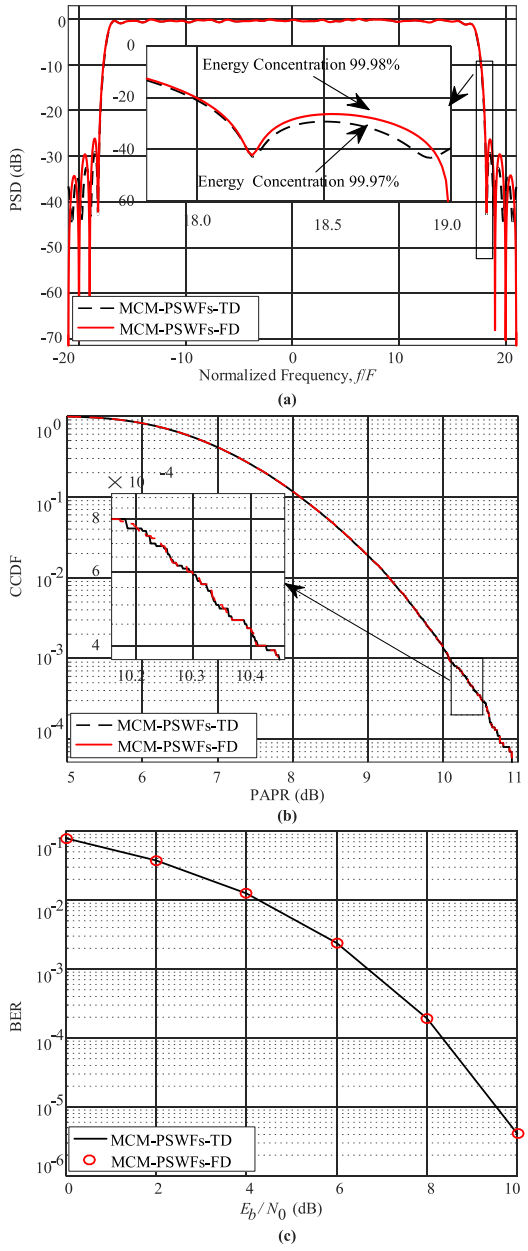

FIGURE 2. The PSD, CCDF and BER performance of MCM-PSWFs-FD and MCM-PSWFs-TD scheme with (a) PSD of modulation signal (b) CCDF of modulation signal (c) BER performance under AWGN channel.

III. PERFORMANCE COMPARISON BETWEEN MCM-PSWFs-FD AND THE OTHER MCM SCHEMES

The MCM-PSWFs-TD scheme realize the signal processing in the time domain. Thus, it is non-trivial to analyze and compare its performance to the benchmarks such as CP-OFDM, WOLA-OFDM, F-OFDM, UFMC, and FBMC-OQAM under the same signal processing framework. However, both the MCM-PSWFs-FD scheme and the aforementioned MCM schemes adopt the IFFT/FFT method. Therefore, it is essential to compare the performance of different schemes. In this section, we provide the comparison and analysis between the proposed MCM-PSWFs-FD scheme and the aforementioned MCM schemes in terms of PSD, SE, BER, PAPR, and computational complexity.

A. PSD OF MODULATION SIGNAL

According to (2) and (6), the PSD of the MCM-PSWFs-FD scheme, denoting as $\mathbf{PSD} \in \mathbb{R}^{N_{\mathrm{FFT}} \times 1}$, can be calculated as follow

$$[\mathbf{PSD}]_k = \sum_{q=1}^{Q} \left| [\mathbf{W}_{N_{FFT}} \mathbf{G} \mathbf{U} \sqrt{\Lambda}]_{q,k} \right|^2, \tag{14}$$

where $\mathbf{W}_{N_{\mathrm{FFT}}}$ represents the DFT matrix of size N_{FFT}, and $\mathbf{U}, \Lambda$ denotes the eigenvectors and eigenvalue matrices of cross-correlation matrix $\mathbf{R_x} = E\{\mathbf{x}\mathbf{x}^{\mathrm{H}}\} = \mathbf{U}\Lambda\mathbf{U}^{\mathrm{H}}$, respectively.

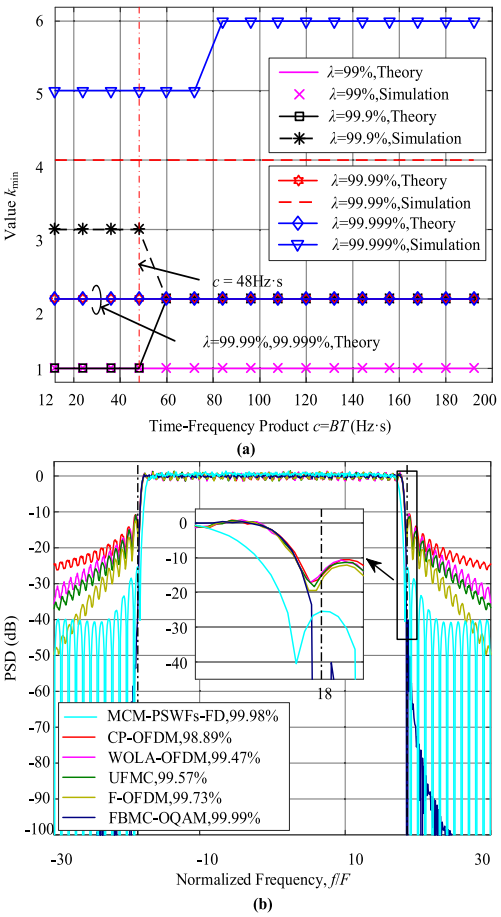

FIGURE 3. The value k_{min} and PSD of modulation signal with (a) k_{min} for different time-frequency product (b) PSD of different modulation signals.

In the condition that the value of time-bandwidth product varies, Fig. 3(a) characterizes the values of numerical k_{min} vs the EC ratio of the MCM-PSWFs-FD signal. Particularly, Fig. 3(a) shows that the EC ratio of modulation signal increases continuously as the number of the PSWFs signals decreases. More particularly, when the measured value k_{min} is 1, 2, 4, the EC ratio of modulation signal is 99%, 99.9% and 99.99%, respectively, under the condition that $c = 48\mathrm{Hz} \cdot \mathrm{s}$. However, a certain gap appears between the

theoretical value and the measured value of k_{min}. For instance, when $c = 48\text{Hz} \cdot \text{s}$, $\lambda = 99.9\%$, the theoretical value of k_{min} is 1 while the measured value is 3. The reason is that the PSWFs signals has no closed-form/analytical expression, its numerical solution is affected by solution method selection, computer truncation and rounding error. Thus, the numerical solution has a certain degree of distortion compared to the theoretical value. And this is one of the reasons why we conducted numerical analysis in Section IV.

When the bandwidth is 0.54 MHz while the subcarrier spacing is $F = 15$ kHz, we have $c = 36\text{Hz} \cdot \text{s}, k = 3$. In order to guarantee the orthogonality (the signal-noise-interference-ratio is more than 65dB) between subcarriers of the WOLA-OFDM, F-OFDM and UFMC scheme, the parameter is settled as $FT_{WOLA} = FT_{F-OFDM} = FT_{UFMC} = 1.09$ [32], where we have $FT_{WOLA} = F(1/F + T_{CP} + T_W)$, $FT_{F-OFDM} = F(1/F + T_{CP} + T_F)$, $FT_{UFMC} = F(1/F + T_{CP} + T_U)$, and T_{CP} represents the CP length, T_W denotes the window function length of WOLA-OFDM, T_F, T_U are the filter length of F-OFDM and UFMC, respectively. Fig. 3(b) illustrates the PSD of different MCM schemes. We can observe from Fig. 3(b) that the EC ratio of the MCM-PSWFs-FD signal is 99.98%, which is higher than CP-OFDM (98.89%), WOLA-OFDM (98.89%), F-OFDM (99.47%), UFMC (99.57%), and lower than the FBMC-OQAM signal (99.99%).

According to the above analysis, the MCM-PSWFs-FD scheme can guarantee that the modulation signal has a higher EC ratio than the benchmarks by controlling the number of PSWFs signals invoked for information transmission. Additionally, the EC ratio of the MCM-PSWFs-FD signals increases continuously as the number of PSWFs signals descends.

B. SPECTRAL EFFICIENCY

Assume that the number of available resource blocks is L, and the number of available carriers in each resource block is N_{RB}. According to the basic principles of QAM and PAM modulation, the QAM constellation can be decomposed into two mutually orthogonal PAM constellations, thus, the MCM-PSWFs-FD scheme can adopt QAM constellation. Therefore, in the condition that the number of symbol periods is Q and the modulation symbol (QAM) is M-ary, the SE of different modulation methods can be uniformly expressed as

$$\eta = \frac{QN'_c \log_2 M}{(QT + T_G + T_T)((LN_{RB} + 1)F + F_G)}, \tag{15}$$

where T represents the time width of the modulation signal, F denotes the subcarrier spacing, T_G indicates the required guard time, F_G qualifies the required guard band, $T_T = (K - 1/2)T$ is the ramp down time of the FBMC-OQAM scheme, K denotes the overlapping factor. Furthermore, N'_c represents the number of signals invoked for information transmission. For the CP-OFDM, WOLA-OFDM, F-OFDM, UFMC, and FBMC-OQAM scheme, the number of signals satisfies $N'_c = N_c = LN_{RB}$; for the MCM-PSWFs-FD scheme, the number of signals satisfies $N'_c = N_c - k, k \geqslant k_{\min}$. According to (15), the SE of the MCM-PSWFs-FD scheme is independent from the number of transmission symbol periods while it increases as N'_c augments.

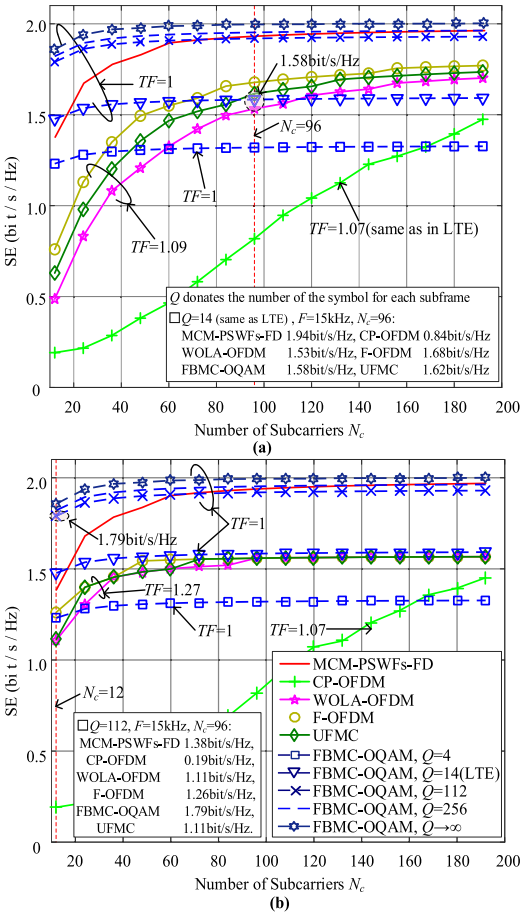

FIGURE 4. The Spectral efficiency of different modulation scheme with (a) when subcarrier spacing $F = 15$ kHz (b) when subcarrier spacing $F = 120$ kHz.

Fig. 4 characterizes the SE of the system over different number of subcarrier. The CP-OFDM, WOLA-OFDM, F-OFDM, UFMC, and FBMC-OQAM scheme are also demonstrated as benchmarks. We can observe from Fig. 4 that the MCM-PSWFs-FD scheme outperforms the benchmarks in terms of the SE under the condition that 99.9% of the transmitted energy is within the bandwidth $(N_c + 1)F + F_G$. To be more precise, when $M = 4$, $N_c = 96$, the SE of the MCM-PSWFs-FD scheme is 1.94 bit/s/Hz, while that is 0.84 bit/s/Hz for the CP-OFDM scheme, 1.75 bit/s/Hz for the WOLA-OFDM scheme, and 1.78 bit/s/Hz for the F-OFDM and UFMC scheme. Meanwhile, the SE of the MCM-PSWFs-FD scheme is larger than that of the FBMC-OQAM scheme when the number of transmission symbol periods Q is small. However, the SE of the FBMC-OQAM scheme will surpass that of the MCM-PSWFs-FD scheme when $Q \to \infty$.

According to the above analysis, it is shown that the MCM-PSWFs-FD scheme has a better SE performance than the CP-OFDM, WOLA-OFDM, F-OFDM, and UFMC scheme. Additionally, compared to the FBMC-OQAM scheme, the MCM-PSWFs-FD scheme outperforms the FBMC-OQAM scheme when the number of transmission symbol periods is small, which indicates that the MCM-PSWFs-FD scheme is more suitable for short-packet communication such as internet of tings (IoT), etc. in terms of SE of the system. It is worth noting that the FBMC-OQAM scheme can strike higher SE than the MCM-PSWFs-FD scheme in the condition that the number of transmission symbol period is large.

C. BER PERFORMANCE

According to (6), at the receiving terminal, the detection statistics $\mathbf{y} \in \mathbb{C}^{Q(\sum_L c_l - k_l)\times 1}$ of the MCM-PSWFs-FD scheme can be expressed as

$$\mathbf{y} = \mathbf{G}^{\mathrm{H}}\mathbf{W}_{N_{FFT}}\mathbf{r} = \mathbf{G}^{\mathrm{H}}\mathbf{H}\mathbf{G}\mathbf{x} + \mathbf{n}, \tag{16}$$

where $N_{FFT} = N_F, \mathbf{H} \in \mathbb{C}^{N_F\times N_F}$ represents the time-variant convolution matrix of the doubly-selective channel, $\mathbf{r} \in \mathbb{C}^{N_F\times 1}$ denotes the sampled received signal and $\mathbf{n} \sim N(0, P_n\mathbf{G}^{\mathrm{H}}\mathbf{G})$ represents the Gaussian distributed noise, with P_n is the white Gaussian noise power in the time domain. Since the wireless channels are highly underspread, the channel induced interference can be neglected compared to the noise interference, which indicates that the off-diagonal elements of $\mathbf{G}^{\mathrm{H}}\mathbf{H}\mathbf{G}\mathbf{x}$ can be neglected [32], [33]. Meanwhile, since the PSWFs signals are orthogonal between each other, i.e., $\mathbf{G}^{\mathrm{H}}\mathbf{G} = \mathbf{I}_{Q(\sum_L c_l - k_l)\times 1}$, thus, (16) can be simplified as

$$\mathbf{y} \approx \mathrm{diag}[\mathbf{H}]\mathbf{x} + \mathbf{n}. \tag{17}$$

Since the MCM-PSWFs-FD scheme adopt QAM constellation, thus, the minimum Euclidean distance of the MCM-PSWFs-FD scheme is the same as the QAM scheme. Therefore, the BER performance of the MCM-PSWFs-FD scheme is the same as the MCM schemes, such as the CP-OFDM, WOLA-OFDM, F-OFDM, UFMC, and FBMC-OQAM scheme, which adopt the QAM scheme.

Correspondingly, in the condition of AWGN channel, $\mathbf{H} = \mathbf{I}_{N_F\times N_F}$, the BER of the MCM-PSWFs-FD scheme can be expressed as [34]

$$P_b = \frac{2/\sqrt{M}}{\log_2\sqrt{M}} \sum_{k=1}^{\log_2\sqrt{M}} \sum_{i=0}^{\left[(1-2^{-k})\sqrt{M}-1\right]} \times \left\{ \begin{array}{l} (-1)^{\left\lfloor \frac{i2^{k-1}}{\sqrt{M}} \right\rfloor} \left(2^{k-1} - \left\lfloor \frac{i2^{k-1}}{\sqrt{M}} + \frac{1}{2} \right\rfloor\right) \\ \times Q\left(\sqrt{\frac{3\log_2 M}{2(M-1)}\frac{E_b}{N_0}}\right) \end{array} \right\}. \tag{18}$$

In the condition of doubly selective channel, $\mathbf{n}/\mathrm{diag}[\mathbf{H}]$ still obeys the Gaussian distribution. When the channel state information (CSI) is perfectly known, the BER of the MCM-PSWFs-FD scheme is given by [33]

$$P_b = \frac{1}{L}\sum_{l=1}^{L}\frac{1}{\log_2 M}\sum_{p=1}^{\log_2 M}\frac{1}{M}\cdot\sum_{j=1}^{M}\sum_{a_v\in\xi_j^p} \Pr\{\hat{x}_{q,l,i} = a_v | x_{q,l,i} = a_j\}, \tag{19}$$

where ξ_j^p represents all those elements of M-ary modulation symbol for which the bit-value at bit position $p \in \mathbb{N}$ is different from the corresponding bit-value of a_j, and $\Pr\{\cdot\}$denotes the probability expression which can be straightforwardly calculated by the cumulative distribution function.

D. PEAK-TO-AVERAGE POWER RATIO

The definition of PAPR for the MCM-PSWFs-FD signal can be expressed as

$$PAPR = \max|s_q(t_h)|^2 / E\left[|s_q(t_h)|^2\right]. \tag{20}$$

Meanwhile, according to (5), the variance of the h-th MCM-PSWFs-FD signal sampling point $s_q[h] = s_q(t_h)$ can be calculated as

$$\begin{aligned} E\left\{s_q[h]s_q^*[h]\right\} &= \frac{T}{\Delta t}E\left[\sum_{p=-BT/2}^{BT/2}\left|\sum_{l=1}^{L}\sum_{i=0}^{c_l-k_l-1} a_{l,p,i}x_{q,l,i}\right|^2\right] \\ &= \frac{T}{\Delta t}E\left[\sum_{p=-BT/2}^{-BT/2}\left|a_p\right|^2\right], \end{aligned} \tag{21}$$

where a_p represents the coefficient of $s_q[h]$ at frequency p/T. The corresponding CCDF of the MCM-PSWFs-FD signal can be expressed as

$$CCDF_{\mathrm{PAPR}}(\xi) = \Pr(\mathrm{PAPR} \geqslant \xi) = 1 - \prod_{i=1}^{\gamma_L}(1 - e^{-\alpha_m\xi^2}), \tag{22}$$

where $\alpha_m = \sigma_x^2/E\left\{s_q[h]s_q^*[h]\right\}$, σ_x^2 represents the variance of the modulation symbol $x_{q,l,i}$.

We can observe from (21) and (22) that, in the condition that the power of modulation signal is constant, the PAPR is closely related to the coefficient $|a_p|$. Denote the average power of the MCM-PSWFs-FD signal as P. Since the CP-OFDM, WOLA-OFDM, F-OFDM and UFMC scheme invoke CP, window function or filter function, different symbol period signals of the FBMC-OQAM scheme overlaps in the time domain, the average power in single symbol period of the aforementioned MCM schemes is $(1+\beta)P$, $\beta \geqslant 0$, which is larger than that of the MCM-PSWFs-FD scheme. It is worth noting that the value β of different MCM schemes varies, which has to be calculated according to specific parameters.

Therefore, when the available resource in the frequency domain is LN_{RB}, the value $|a_p|$ of different modulation schemes has to obey the following relationship $|a_p^{\text{MCM - PSWFs - FD}}| = P/LN_{RB} < |a_p^{\text{Others}}| = (1+\beta)P/LN_{RB}$, which indicates that the MCM-PSWFs-FD scheme outperforms the benchmarks in terms of the PAPR performance.

TABLE 1. The computational complexity of different modulation schemes.

Modulation Scheme	Complexity (CMs)
MCM-PSWFs-FD	$N_c(N_c-k)+XN_c\log_2 XN_c$
CP-OFDM	$XN_c\log_2 XN_c$
WOLA-OFDM	$XN_c\log_2 XN_c+2N_W$
F-OFDM	$XN_c\log_2 XN_c+2N_F(XN_c+N_{CP}+1)$
UFMC	$(XN_c\log_2 XN_c+2N_U(XN_c+N_{CP}+1))g$
FBMC-OQAM	$KXN_c\log_2 XN_c+2KXN_c$

E. COMPUTATIONAL COMPLEXITY

The computational complexity of different MCM schemes is analyzed in terms of the CMs, which is demonstrated in Table 1. Here, N_c represents the number of carrier, X denotes the oversampling multiple of the modulation signal, N_{CP} indicates the number of sampling points in the CP, N_W is the number of sampling points in the window function adopted by the WOLA-OFDM scheme, N_F, N_U are the number of sampling points in the filter function adopted by the F-OFDM scheme and the UFMC scheme, g denotes the number of sub-bands of the UFMC scheme. We can observe from Table 1 that the relationship of computational complexity between the MCM-PSWFs-FD scheme and the CP-OFDM, WOLA-OFDM, F-OFDM, UFMC, FBMC-OQAM scheme is related to the oversampling multiple X. Especially, when $X\log_2 XN_c, N_F, N_U \rightarrow N_c$, the computational complexity of the MCM-PSWFs-FD scheme is $O(N_c\log_2 N_c)$, which is similar to that of the CP-OFDM, WOLA-OFDM and FBMC-OQAM scheme while lower than that of the F-OFDM and UFMC scheme.

In summary, at the cost of increasing the computational complexity, which is affordable due to the development of hardware techniques, the MCM-PSWFs-FD scheme is capable of reaping the following advantages:

1) Compared to the CP-OFDM, WOLA-OFDM, F-OFDM and UFMC scheme, it can obtain a higher EC and SE while a lower PAPR.

2) Compared to the FBMC-OQAM scheme, it can attain a lower PAPR while strike a higher SE in the condition that the number of transmission symbol period is small. It is worth noting that the FBMC-OQAM scheme outperforms the MCM-PSWFs-FD scheme in term of the PSD properties, while strike a higher SE in the condition that the number of transmission symbol period is large.

IV. NUMERICAL ANALYSIS

In this section, in order to accurately analyze the system performance of the MCM-PSWFs-FD scheme, we provide the numerical results in terms of PSD, PAPR, adjacent frequency band interference, and BER performance for validating our analysis and for further comparing the performance between the MCM-PSWFs-FD scheme and the benchmarks.

A. PARAMETERS FOR SIMULATION

Our simulation parameters are given in Table 2. Assume that the available time width is $T = 10/F_1$, there are two adjacent frequency bands B_1, B_2, whose bandwidth is 1.44 MHz. Finally, the subcarrier spacing is $F_1 = 15$ kHz, $F_2 = 120$ kHz, respectively. In order to guarantee the orthogonality between subcarriers of the WOLA-OFDM, F-OFDM and UFMC scheme, we set the parameter as $T_1F_1 = 1.09$, $T_2F_2 = 1.27$ [32], respectively.

TABLE 2. Simulation parameters [32].

Overall parameters		
Bandwidth /MHz	B	1.44
Subcarrier spacing /kHz	F_1	15
	F_2	120
Bit per symbol	$\log_2 M$	2
Oversampling multiple	X	14
Channel condition	AWGN, Flat-fading and doubly-selective channels	
CP-OFDM parameters (same as in LTE)		
Cyclic prefixs /μs	$T_{CP,15}$	4.76
	$F_{CP,120}$	0.60
FBMC-OQAM parameters		
Overlapping factor	K	4
WOLA-OFDM parameters		
Cyclic prefix /μs	$T_{CP,15}$	3.00
	$F_{CP,120}$	1.13
Window length /μs	$T_{W,15}$	3.00
	$F_{W,120}$	1.13
F-OFDM parameters		
Cyclic prefix /μs	$T_{CP,15}$	6.00
	$F_{CP,120}$	2.25
Window length /μs	$T_{F,15}$	5.62
	$F_{F,120}$	1.79
UFMC parameters		
Cyclic prefix /μs	$T_{CP,15}$	6.00
	$F_{CP,120}$	2.25
Window length /μs	$T_{U,15}$	4.76
	$F_{U,120}$	2.25
MCM-PSWFs-FD parameters		
Time-frequency product /Hz · s	c_1	96
	c_2	12
Sampling points in frequency domain	N_F	c_1, c_2
EC ratio	99.9%	
Value k	k_1	2
	k_2	3

B. SIMULATION RESULTS AND ANALYSIS

1) PSD OF THE MODULATION SIGNAL

Fig. 5 characterizes the PSD of the modulation signal over different MCM schemes. We can observe from Fig. 5 that the first sidelobe of the MCM-PSWFs-FD signal is lower than that of the CP-OFDM, WOLA-OFDM, F-OFDM and UFMC signal while higher than that of the FBMC-OQAM signal. Corresponding, the EC of the MCM-PSWFs-FD signal is higher than that of the CP-OFDM, WOLA-OFDM, F-OFDM and UFMC signal while lower than that of the FBMC-OQAM signal. Moreover, by further combining with Fig. 3 and Fig. 4, it is demonstrated that in the condition of the same EC ratio (99.9%) while $F_1 = 15$ kHz and $Q = 14$, compared to the CP-OFDM, WOLA-OFDM, F-OFDM, UFMC and FBMC-OQAM scheme, the SE of the MCM-PSWFs-FD scheme is improved by about 1.1, 0.19, 0.16, 0.16, 0.36 (bit/s/Hz), respectively. But the SE of the FBMC-OQAM

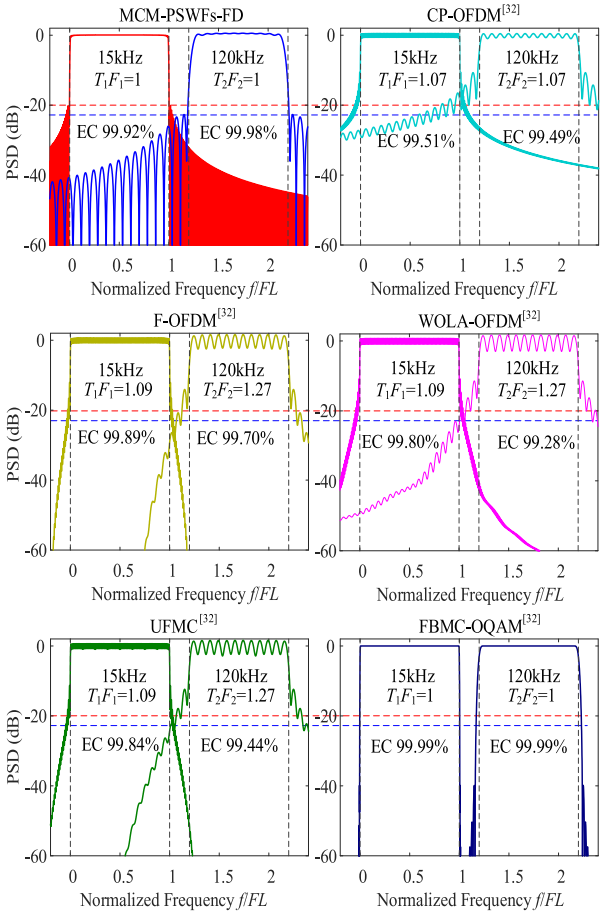

FIGURE 5. The PSD of different modulation signal with different subcarrier spacings($F_1 = 15$ kHz, $F_2 = 120$ kHz).

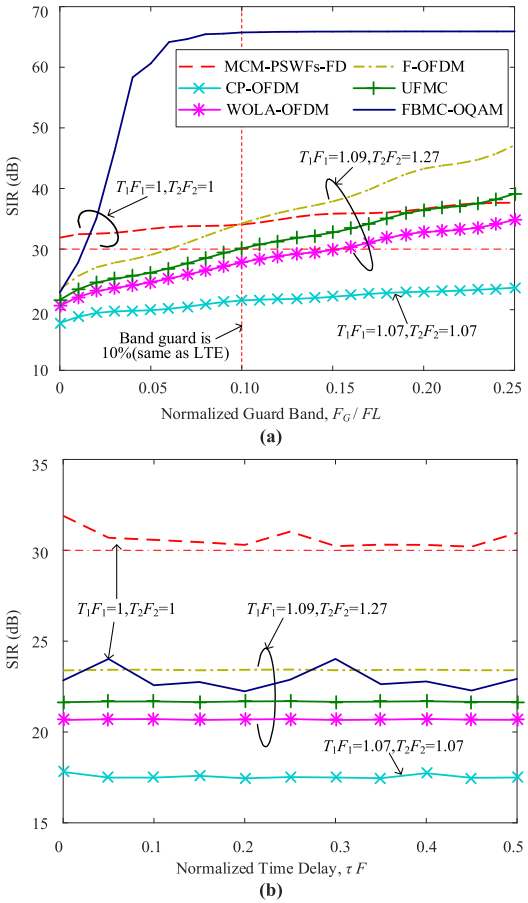

FIGURE 6. The SIR of different modulation signal in case that two users with different subcarrier spacings share the same band with (a) when delay $\tau = 0$ (b) when guard band $F_G = 0$.

scheme is 1.79 bit/s/Hz in the condition that $F_2 = 120$ kHz and $Q = 112$, which is higher than the MCM-PSWFs-FD scheme (1.38 bit/s/Hz).

The above analysis indicates that the MCM-PSWFs-FD signal has the advantage of high energy concentration. Meanwhile, it can guarantee that the modulation signal with high energy concentration by simply controlling the number of the PSWFs signals invoked for information transmission, which is capable of striking a tradeoff between the energy concentration and SE. Finally, all the simulation results coincide with the corresponding theoretical results.

2) SIGNAL TO INTERFERENCE RATIO OF ADJACENT SUB-BANDS

We consider the signal to interference ratio (SIR) [32] as the measurement criteria for analyzing the interference between adjacent frequency bands over different modulation schemes. We can observe from Fig. 6 that, when the time delay is 0, the SIR between the MCM-PSWFs-FD signals is higher than 30 dB under different guard band. When the guard band is small, the SIR of the MCM-PSWFs-FD signals is higher than that of the CP-OFDM, WOLA-OFDM, F-OFDM, UFMC, and FBMC-OQAM signals. However, when the guard band is large, the SIR of the aforementioned MCM schemes will be higher than that of the MCM-PSWFs-FD scheme, especially for FBMC-OQAM. To be more precise, when the normalized guard band is 10% (same as LTE), the SIR of the FBMC-OQAM scheme is 65.7 dB, which is higher than the MCM-PSWFs-FD scheme (34.3 dB). This is due to that the PSWFs signals are multi-frequency signals, the spectrums of different order PSWFs signals in the same sub-band are completely overlapped, thus, the different order PSWFs signals in adjacent sub-bands will interfere with each other. Additionally, when the guard band is 0, the SIR of the MCM-PSWFs-FD signals is higher than 30 dB over different delays while it is higher than that of the CP-OFDM, WOLA-OFDM, F-OFDM, UFMC, and FBMC-OQAM signals. The above analysis indicates that the MCM-PSWFs-FD signal is capable of obtaining a lower adjacent frequency band interference and it is more suitable for asynchronous communication. Meanwhile, it also reveals that the MCM-PSWFs-FD signal is capable of attaining high energy concentration.

3) PAPR OF THE MODULATION SIGNAL

The CCDF of the MCM-PSWFs-FD signal is illustrated in Fig. 7(a). It demonstrates that the PAPR of the

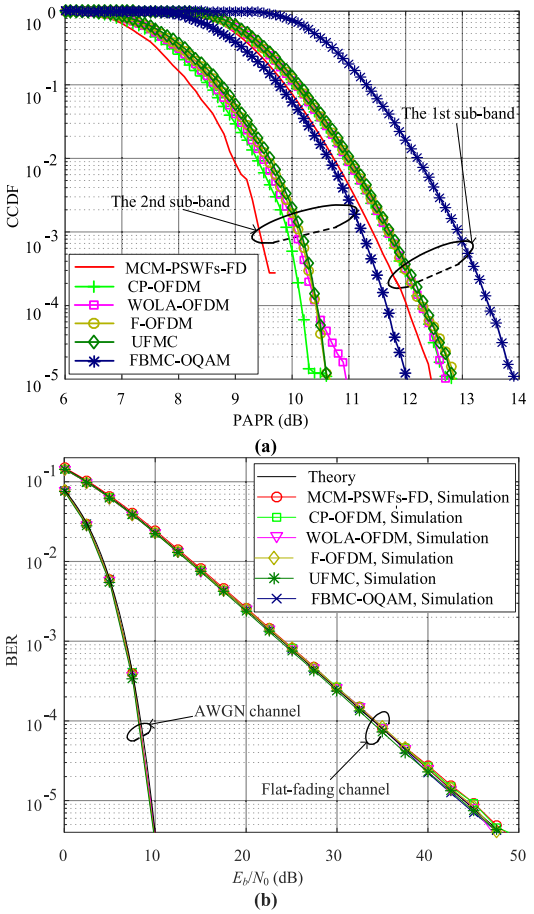

FIGURE 7. The CCDF and BER performance of different modulation schemes with (a) CCDF of different modulation signal with different subcarrier spacings (b) BER performance of different modulation schemes under AWGN channel and flat-fading channel.

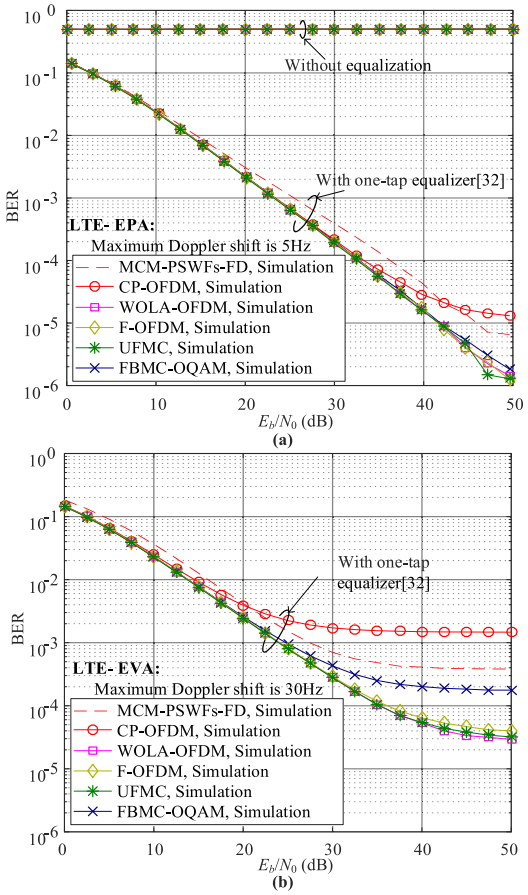

FIGURE 8. The BER performance of MCM-PSWFs-FD under doubly-selective channels with (a) EPA, 5 Hz (b) EVA, 30 Hz.

MCM-PSWFs-FD signal is lower than that of the CP-OFDM, WOLA-OFDM, F-OFDM, UFMC and FBMC-OQAM signal, which coincide with the corresponding theoretical results.

4) BER PERFORMANCE

Fig. 7(b) characterizes the BER performance of the MCM-PSWFs-FD scheme in the conditions of AWGN channel and Flat-fading channel (CSI is perfectly known). We can observe from the simulation results that the BER performance of the MCM-PSWFs-FD scheme is the same as that of the CP-OFDM, WOLA-OFDM, F-OFDM, UFMC and FBMC-OQAM scheme, which also coincide with the corresponding theoretical results.

Fig. 8 and Fig. 9 characterizes the BER performance of the MCM-PSWFs-FD scheme in the conditions of doubly-selective channels. We can observe from the simulation results that under doubly-selective channels, without using equalization processing, the BER performance of the MCM-PSWFs-FD scheme is very poor, and the simple one-tap equalizer [32] can effectively improve the BER performance, as shown in Fig. 8(a). Meanwhile, Fig. 8(b) and Fig. 9(a) demonstrates that the BER performance of the MCM-PSWFs-FD scheme is better than CP-OFDM in the conditions that the Doppler shift is small, such as in the extended pedestrian A model (EPA, 5 HZ) and extended vehicular A model (EVA, 30 km/h, 100 km/h) of LTE. But the BER performance of the MCM-PSWFs-FD scheme is lower than CP-OFDM in the conditions that the Doppler shift is large, such as in the EVA (500 km/h).

It is worth noting that under the conditions of doubly-selective channels, the BER performance of the MCM-PSWFs-FD scheme is lower than WOLA-OFDM, F-OFDM, UFMC, and FBMC-OQAM. The reason is that there is no cyclic prefix, and the PSWFs signals are multi-frequency signals, the spectrums of different order PSWFs signals in the same sub-band are completely overlapped. Under the EPA and EVA channels, when the multiple-path interference and Doppler frequency shift exists simultaneously, not only the PSWFs signals in the same frequency band interfere with each other, but also the PSWFs signals in adjacent frequency bands also have interference. Therefore, compared to F-OFDM, UFMC, WOLA-OFDM, FBMC-OQAM, the interference between the signals of MCM-PSWFs-FD is more serious, and the BER performance of the MCM-PSWFs-FD scheme is lower than the above

TABLE 3. Key system performance indicators of different modulation schemes with parameters in Table 2.

Modulation Schemes	EC ratio (%) in Design Bandwidth		SE (bit/s/Hz) EC ratio is 99.9%		PAPR (dB) CCDF=10^{-3}		CMs	SIR (dB) $\tau = 0, F_G = 0.1 * FL$ (same as LTE)
	15kHz	120kHz	15kHz	120kHz	15kHz	120kHz		
MCM-PSWFs-FD	99.92	99.98	1.94	1.38	11.4	9.5	6.8×10^5	34.3
CP-OFDM	99.51	97.49	0.84	0.19	11.7	9.9	4.8×10^5	21.5
WOLA-OFDM	99.80	99.28	1.53	1.11	11.7	10.1	4.9×10^5	27.7
F-OFDM	99.89	99.70	1.68	1.26	11.7	10.1	5.5×10^6	34.3
UFMC	99.84	99.44	1.62	1.11	11.7	10.1	2.9×10^7	30.1
FBMC-OQAM	99.99	99.99	1.58	1.79	12.9	11.2	7.0×10^5	65.7

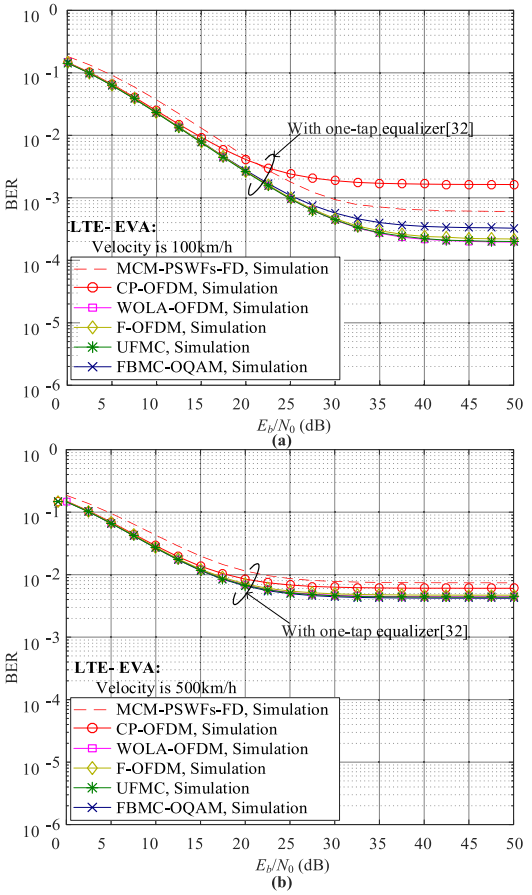

FIGURE 9. The BER performance of MCM-PSWFs-FD under doubly-selective channels with (a) EVA, 100 km/h (b) EVA, 500 km/h.

modulation method. Although the aforementioned MCM scheme performs better under doubly-selective channels, the proposed MCM-PSWFs-FD has other advantages, such as the MCM-PSWFs-FD scheme is capable of striking a favorable tradeoff between the computational complexity and the system performance, while the signal waveform design is also more concise and flexible. Furthermore, the simple one-tap equalizer is adopted in this paper. If the characteristics of the MCM-PSWFs-FD signals are considered, a more reasonable equalizer is designed, which is expected to further improve the BER performance of the MCM-PSWFs-FD at the cost of increasing the complexity of equalization processing.

C. POSSIBLE USE CASE FOR MCM-PSWFs-FD

Based on the related analysis in Section III and Section IV, the key system performance indicators of different MCM schemes are illustrated in Table 3 under the same simulation conditions with Table 2. Through comparative analysis, it is found that the advantages and disadvantages of the proposed MCM-PSWFs-FD scheme compared to the benchmarks are as follows:

1) Compared to the CP-OFDM, WOLA-OFDM, F-OFDM, and UFMC schemes, the signal waveform design of the MCM-PSWFs-FD scheme is more concise and flexible, with higher EC and SE, lower adjacent frequency band interference and PAPR.

2) Compared to the FBMC-OQAM scheme, it can attain a lower PAPR while strike a higher SE in the condition that the number of transmission symbol period is small. But the FBMC-OQAM scheme can attain a higher EC, lower adjacent frequency band interference while strike a higher SE in the condition that the number of transmission symbol period is large.

3) Because there is no cyclic prefix and the PSWFs signals are multi-frequency signals, the proposed MCM-PSWFs-FD scheme is severely affected by multipath and Doppler frequency shifts. Therefore, the MCM-PSWFs-FD scheme needs to adopt signal equalization processing to improve BER performance.

According to the above advantages and disadvantages of the MCM-PSWFs-FD scheme, it has the following possible applications:

a) **Dynamic spectrum sharing:** Due to the randomness of the size, frequency band, bandwidth, time width and type of the idle time-frequency resources, dynamic spectrum sharing requires flexible signal waveform design, which can flexibly design signal waveforms based on the available time-frequency resources.

When the spectrum range is $[f_L, f_H]$ (Hz), the bandwidth is $B = f_H - f_L$ (Hz), and the time width is T (s), the PSWFs as a special class of non-sinusoidal signals, its integral equation can be expressed as

$$\int_{-T/2}^{T/2} \varphi_n(c,\tau) \left[\frac{\frac{\sin f_H(t-\tau)}{\pi(t-\tau)} - }{\frac{\sin f_L(t-\tau)}{\pi(t-\tau)}} \right] d\tau = \varphi_n(c,t)\lambda_n, \quad (23)$$

where $\varphi_n(c,t)$ denotes the n-th PSWFs, whose time-frequency product is $c = BT$(Hz · s). λ_n represents the

eigenvalue of $\varphi_n(c,t)$, which reflects the energy concentration of PSWFs signal. The larger λ_n is, the better the energy concentration of $\varphi_n(c,t)$ is, and λ_n decreases as the signal order n increases. It is worth noting that the PSWFs signals is baseband and $n \in [0, \lfloor c-1 \rfloor]$ when $f_L = 0$ Hz, the PSWFs signals is pass band and $n \in [0, \lfloor 2c-1 \rfloor]$ when $f_L > 0$ Hz.

According to (23), the PSWFs with different bandwidths, frequency ranges, and time widths can be generated by changing the parametersf_L, f_H (Hz) and parameter T (s) in the PSWFs integral equation. Therefore, in engineering applications, the corresponding PSWFs signals can be directly generated according to the available time-frequency resources, which indicates that the PSWFs waveform design is very simple and flexible.

In addition, in order to guarantee the energy concentration of the modulation signal and the PSWFs signals of adjacent sub-bands are orthogonal to each other, in the MCM-PSWFs-FD scheme, only the former $\lfloor c-k \rfloor$ order PSWFs signals are selected for information transmission, where k is a positive integer. Therefore, the MCM-PSWFs-FD scheme can strike a higher SE in the condition that the size of the idle time-frequency resources are large, and attain a higher energy concentration at the expense of SE. However, the waveform design of the MCM-PSWFs-FD scheme is more concise and flexible.

b) **eMBB and mMTC:** 5G is expected to enhance three major application scenarios: enhanced mobile broadband (eMBB), ultra-reliable and low latency communications (uRLLC) and massive machine-type communications (mMTC). Among them, uRLLC needs to support low latency and high reliability. Since there is no cyclic prefix and the PSWFs signals are multi-frequency signals, the MCM-PSWFs-FD scheme needs to increase the time width and adopt equalization processing to resist multipath and Doppler frequency shift interference and improve the BER performance. However, the above processing will increase the latency. Therefore, the MCM-PSWFs-FD scheme is not suitable for uRLLC.

Unlike uRLLC, eMBB and mMTC have low latency requirements. Therefore, MCM-PSWFs-FD can be applied to eMBB and mMTC. The eMBB with large available bandwidth have high information transmission rate requirements, and the MCM-PSWFs-FD scheme can strike high SE in the condition that the size of the available bandwidth is large while can effectively improve the BER performance by equalization processing.

The mMTC have massive and asynchronous access requirements, supporting different types of equipment for asynchronous communication, but have low information transmission rate requirements. It indicates that the MCM-PSWFs-FD scheme can increase the time width and adopt equalization processing to improve the BER performance.

In addition, due to the MCM-PSWFs-FD scheme is more concise and flexible, with higher EC and SE, lower adjacent frequency band interference, different orders of PSWFs signals are orthogonal to each other, it can provide a variety of

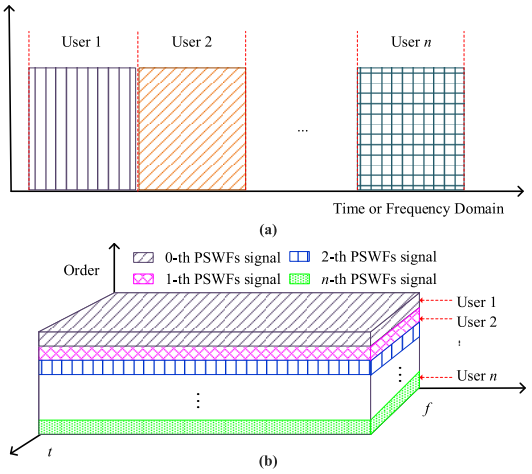

FIGURE 10. Multiple access scheme of MCM-PSWFs-FD with (a) frequency division and time division multiple access (b) code division multiple access.

flexible access for mMTC and increase access capacity. For example, when multiple different types of users or devices are required to access at the same time in mMTC, the frequency division and time division multiple access can be used for the users or devices that cannot fully guarantee synchronization which is illustrated in Fig.10(a), and the code division multiple access based on the order of the PSWFs signal for the users or devices that are easy to achieve synchronization which is illustrated in Fig.10(b). It is worth noting that the amount of the information transmitted by the device or user is generally small in mMTC scenario, and most are short packet communication, that is, the number of transmission symbol period is small. Therefore, the MCM-PSWFs-FD scheme can strike a higher SE than FBMC-OQAM, which is more suitable for mMTC in terms of SE of the system.

However, the MCM-PSWFs-FD scheme needs to perform equalization processing to improve the BER performance in the conditions of doubly-selective channels, which will cause the complexity of the receiving system to increase, especially when the BER performance is seriously affected by the channel.

V. CONCLUSION

In this paper, we proposed a novel MCM-PSWFs-FD scheme for reducing the computational complexity of the MCM-PSWFs-TD scheme by constructing the relationship between the discrete representation and exponential function representation of the MCM-PSWFs-TD signals, and switching the signal processing from the time domain to the frequency domain. Compared to the conventional MCM-PSWFs-TD scheme, the proposed scheme invoked only signal waveform of the half spectrum range for information loading and signal detection in the frequency domain. This concept can not only significantly reduce the computational complexity without severely degrading the system performance, but also leverage the IFFT/FFT method, which can be adopted in the application such as Wi-Fi, LTE and 5G.

Additionally, the CP-OFDM, WOLA-OFDM, F-OFDM, UFMC and FBMC-OQAM scheme are also demonstrated as benchmarks. Compared to the benchmark MCM schemes, the waveform design of the MCM-PSWFs-FD scheme is more concise and flexible while the MCM-PSWFs-FD scheme is capable of striking tradeoffs among SE, OOB energy leakage, adjacent frequency band interference, PAPR, and the computational complexity. It is worth noting that the FBMC-OQAM scheme shows better performance than the proposed MCM-PSWFs-FD schemes. However, the MCM-PSWFs-FD scheme is expected to provide a flexibility and high efficiency signal waveform for the Wi-Fi, LTE, 5G and B5G communication systems by enabling flexible allocation and dynamic sharing of different type of time-frequency resources, which in turn, improves the SE and NR flexibility.

REFERENCES

[1] S.-Y. Lien, S.-L. Shieh, Y. Huang, B. Su, Y.-L. Hsu, and H.-Y. Wei, "5G new radio: Waveform, frame structure, multiple access, and initial access," *IEEE Commun. Mag.*, vol. 55, no. 6, pp. 64–71, Jun. 2017.

[2] Y. Cai, Z. Qin, F. Cui, G. Y. Li, and J. A. McCann, "Modulation and multiple access for 5G networks," *IEEE Commun. Surveys Tuts.*, vol. 20, no. 1, pp. 629–646, 1st Quart., 2018.

[3] Z. Ma, Z. Zhang, Z. Ding, P. Fan, and H. Li, "Key techniques for 5G wireless communications: Network architecture, physical layer, and MAC layer perspectives," *Sci. China Inf. Sci.*, vol. 58, no. 4, pp. 1–20, Feb. 2015.

[4] X. You, C. Zhang, X. Tan, S. Jin, and H. Wu, "AI for 5G: Research directions and paradigms," *Sci. China Inf. Sci.*, vol. 62, no. 2, pp. 551–563, Feb. 2019.

[5] M. Ibrahim, A. F. Demir, and H. Arslan, "Time–frequency warped waveforms," *IEEE Commun. Lett.*, vol. 23, no. 1, pp. 36–39, Jan. 2019.

[6] L. Zhang, Y.-C. Liang, and M. Xiao, "Spectrum sharing for Internet of Things: A survey," *IEEE Wireless Commun.*, vol. 26, no. 3, pp. 132–139, Jun. 2019.

[7] W. Zhang, C.-X. Wang, X. Ge, and Y. Chen, "Enhanced 5G cognitive radio networks based on spectrum sharing and spectrum aggregation," *IEEE Trans. Commun.*, vol. 66, no. 12, pp. 6304–6316, Dec. 2018.

[8] D. Slepian and H. O. Pollak, "Prolate spheroidal wave functions, Fourier analysis, and uncertainty-I," *Bell Syst. Tech. J.*, vol. 40, no. 1, pp. 43–46, Jan. 1961.

[9] M. De Sanctis, E. Cianca, T. Rossi, C. Sacchi, L. Mucchi, and R. Prasad, "Waveform design solutions for EHF broadband satellite communications," *IEEE Commun. Mag.*, vol. 53, no. 3, pp. 18–23, Mar. 2015.

[10] A. Osipov, V. Rokhlin, and H. Xiao, *Prolate Spheroidal Wave Functions of Order Zero*. Boston, MA, USA: Springer, 2013, pp. 33–66.

[11] Z.-Y. Zhao, H.-X. Wang, X.-G. Liu, P.-L. Zhong, Z.-N. Chen, and J.-F. Kang, "Orthogonal prolate spheroidal wave functions pulse modulation method," *J. Electron. Inf. Technol.*, vol. 34, no. 10, pp. 2331–2335, Oct. 2012.

[12] S. Majhi and P. Richardson, "Capacity analysis of orthogonal pulse-based TH-UWB signals," *Wireless Pers. Commun.*, vol. 64, no. 2, pp. 255–272, Dec. 2010.

[13] W. Dullaert, H. Rogier, and F. Boeykens, "Advantages of PSWF-based models for UWB systems," in *Proc. APWC*, Cape Town, South Africa, Oct. 2012, pp. 1024–1027.

[14] Z. Zhao, H. Zhou, Z. Mao, and X. Liu, "Orthogonal carrier modulation based on prolate spheroidal wave function," *Syst. Eng. Electron.*, vol. 36, no. 12, pp. 2533–2537, Dec. 2014.

[15] H.-X. Wang, X.-G. Liu, Z.-Y. Zhao, C.-H. Liu, and Z.-N. Chen, "A method of nonsinusoidal orthogonal modulation in time domain based on ternary coding," *J. Electron. Inf. Technol.*, vol. 33, no. 8, pp. 2003–2007, Aug. 2011.

[16] Z. Chen, H. Wang, Z. Mao, and J. Kang, "A multidimensional constellation demodulation method for broadband satellite communication signals," *Acta Aeronauticaet Astronautica Sinica*, vol. 35, no. 3, pp. 828–837, Mar. 2014.

[17] I. B. Djordjevic, A. Z. Jovanovic, Z. H. Peric, and T. Wang, "Multidimensional optical transport based on optimized vector-quantization-inspired signal constellation design," *IEEE Trans. Commun.*, vol. 62, no. 9, pp. 3262–3273, Sep. 2014.

[18] Z. Chen, H. Wang, X. Liu, and P. Zhong, "Maximal capacity nonorthogonal pulse shape modulation," *Chin. J. Aeronaut.*, vol. 28, no. 6, pp. 1699–1708, Dec. 2015.

[19] F. Lu, H. Wang, C. Liu, Z. Chen, and J. Kang, "Power domain nonorthogonal pulse modulation based on prolate spheroidal wave function," *Acta Aeronauticaet Astronautica Sinica*, vol. 40, no. 9, Sep. 2019, Art. no. 323102.

[20] D. Slepian, "Prolate spheroidal wave functions, Fourier analysis, and uncertainty-V: The discrete case," *Bell Syst. Tech. J.*, vol. 57, no. 5, pp. 1371–1430, May 1978.

[21] J. Kang, H. Wang, F. Lu, and C. Liu, "Strict parity symmetric prolate spheroidal wave functions signal construction and low complexity detection method," *SCIENTIA SINICA Informationis*, vol. 50, no. 5, pp. 766–776, May 2020.

[22] C. Tao and C. Tao, *Optical Information Theory*. Beijing, China: Science Press, 1999, pp. 1–13.

[23] P. Guan, D. Wu, T. Tian, J. Zhou, X. Zhang, L. Gu, A. Benjebbour, M. Iwabuchi, and Y. Kishiyama, "5G field trials: OFDM-based waveforms and mixed numerologies," *IEEE J. Sel. Areas Commun.*, vol. 35, no. 6, pp. 1234–1243, Jun. 2017.

[24] L. Zhang, A. Ijaz, P. Xiao, M. M. Molu, and R. Tafazolli, "Filtered OFDM systems, algorithms, and performance analysis for 5G and beyond," *IEEE Trans. Commun.*, vol. 66, no. 3, pp. 1205–1218, Mar. 2018.

[25] Y. Li, B. Tian, K. Yi, and Q. Yu, "A novel hybrid CFO estimation scheme for UFMC-based systems," *IEEE Commun. Lett.*, vol. 21, no. 6, pp. 1337–1340, Jun. 2017.

[26] S. Buzzi, C. D'Andrea, D. Li, and S. Feng, "MIMO-UFMC transceiver schemes for millimeter-wave wireless communications," *IEEE Trans. Commun.*, vol. 67, no. 5, pp. 3323–3336, May 2019.

[27] H. Jamal and D. W. Matolak, "Dual-polarization FBMC for improved performance in wireless communication systems," *IEEE Trans. Veh. Technol.*, vol. 68, no. 1, pp. 349–358, Jan. 2019.

[28] R. Nissel and M. Rupp, "Pruned DFT-spread FBMC: Low PAPR, low latency, high spectral efficiency," *IEEE Trans. Commun.*, vol. 66, no. 10, pp. 4811–4825, Oct. 2018.

[29] D. Slepian, "Some asymptotic expansions for prolate spheroidal wave functions," *J. Math. Phys.*, vol. 44, nos. 1–4, pp. 99–140, Apr. 1965.

[30] I. Selinis, K. Katsaros, M. Allayioti, S. Vahid, and R. Tafazolli, "The race to 5G era; LTE and Wi-Fi," *IEEE Access*, vol. 6, pp. 56598–56636, Oct. 2018.

[31] A. Hammoodi, L. Audah, and M. A. Taher, "Green coexistence for 5G waveform candidates: A review," *IEEE Access*, vol. 7, pp. 10103–10126, Jan. 2019.

[32] R. Nissel, S. Schwarz, and M. Rupp, "Filter bank multicarrier modulation schemes for future mobile communications," *IEEE J. Sel. Areas Commun.*, vol. 35, no. 8, pp. 1768–1782, Aug. 2017.

[33] R. Nissel and M. Rupp, "OFDM and FBMC-OQAM in doubly-selective channels: Calculating the bit error probability," *IEEE Commun. Lett.*, vol. 21, no. 6, pp. 1297–1300, Jun. 2017.

[34] K. Cho and D. Yoon, "On the general BER expression of one- and two-dimensional amplitude modulations," *IEEE Trans. Commun.*, vol. 50, no. 7, pp. 1074–1080, Jul. 2002.

HONGXING WANG received the B.Eng. degree in telecommunication from the Chengdu Telecommunication Engineering Institute, China, in 1982, the M.Eng. degree in communication and electronic system from Naval Aeronautical and Astronautical Engineering University, China, in 1990, and the Ph.D. degree in communication and information systems from Beijing Aeronautical and Astronautical University, China, in 2007.

He is currently a Full Professor and a Ph.D. Supervisor with the Department of Aeronautical Communication, Naval Aviation University, China. His research interests include modern multicarrier communication systems, digital signal processing, optical wireless communications, and 5G wireless networks.

FAPING LU received the B.S. degree in communication engineering from Nanchang University, China, in 2014, and the M.S. degree in communication and information systems from Naval Aviation Engineering University, China, in 2017. He is currently pursuing the Ph.D. degree with the Department of Aeronautical Communication, Naval Aviation University, China. His current research interests include digital signal processing, modern communication systems, and waveform design for 5G.

CHUANHUI LIU received the B.Eng. degree in aeronautical radio, and the M.Eng. and Ph.D. degrees in communication and information systems from Naval Aeronautical and Astronautical Engineering University, China, in 2005, 2008, and 2013, respectively.

He is currently a Lecturer with the Department of Aeronautical Communication, Naval Aviation University, China. His current research interests include digital signal processing, statistical signal processing for wireless applications, waveform design for 5G, and UWB communication.

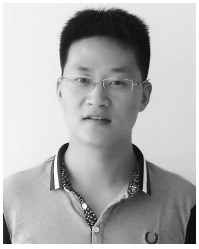

XIAO LIU received the B.S. degree in communication engineering and the M.S. degree in communication and information systems from Naval Aeronautical and Astronautical University, China, in 2009 and 2016, respectively. He is currently pursuing the Ph.D. degree with the Department of Aeronautical Communication, Naval Aviation University, China. His current research interests include modern communication systems and waveform design for 5G.

JIAFANG KANG received the B.Eng. and M.Eng. degrees in information engineering and the Ph.D. degree in communication and information systems from Naval Aeronautical and Astronautical Engineering University, China, in 2008, 2010, and 2014, respectively.

He is currently a Lecturer with the Department of Aeronautical Communication, Naval Aviation University, China. His current research interests include modern multicarrier communications over fading channels, statistical signal processing for wireless applications, and signal design for GNSS.